Hectometer Revivals of Quantum Interference

Markus Rambach,[1,*] W. Y. Sarah Lau,[1] Simon Laibacher,[2] Vincenzo Tamma,[3,2]
Andrew G. White,[1] and Till J. Weinhold[1]

[1]*ARC Centre for Engineered Quantum Systems, School of Mathematics and Physics, University of Queensland, Brisbane, Queensland 4067, Australia*
[2]*Institut für Quantenphysik and Center for Integrated Quantum Science and Technology (IQ[ST]), Universität Ulm, Ulm, Baden-Württemberg 89069, Germany*
[3]*Faculty of Science, SEES and Institute of Cosmology & Gravitation, University of Portsmouth, Portsmouth, Hampshire PO1 2UP, United Kingdom*

Cavity-enhanced single photon sources exhibit mode-locked biphoton states with comblike correlation functions. Our ultrabright source additionally emits single photon pairs as well as two-photon NOON states, dividing the output into an even and an odd comb, respectively. With even-comb photons we demonstrate revivals of the typical nonclassical Hong-Ou-Mandel interference up to the 84th dip, corresponding to a path length difference exceeding 100 m. With odd-comb photons we observe single photon interference fringes modulated over twice the displacement range of the Hong-Ou-Mandel interference.

The Hong-Ou-Mandel (HOM) effect [1–3]—where photons in separate spatial modes coalesce after interfering at a beam splitter—is the most famous signature of nonclassical interference. It varies directly with the indistinguishability of the interacting light fields in all degrees of freedom (d.o.f.). This effect is inherently quantum and foundational in many quantum applications, including photonic entangling gates [4–8], measurement processes [9–11], and boson sampling [12–15], and can also be used to measure the temporal width of the photonic wave packet [2] or perform (sub)femtosecond spectroscopy [16–18]. The result of HOM interference is a low-order NOON state [19,20], which is of great interest in metrology as it has both phase superresolution and phase supersensitivity [21].

The sensitivity of HOM interference to distinguishability in all d.o.f. makes it a useful sensor to detect phase drifts or displacements, e.g., see [22]. Most commonly a decrease in the coincidence rate—a HOM dip—is observed by varying the arrival time of the photons or the path lengths traversed by the light fields. Traditional single photon sources based on atoms, quantum dots, or parametric down-conversion will exhibit a single dip with a width representative of the coherence time of the two-photon state, usually on the order of picoseconds to femtoseconds.

Lu, Campbell, and Ou [23] showed that placing a cavity before the interfering beam splitter leads to *revivals* of the HOM interference, spaced by the round trip time of the cavity. The photons are then generated in a mode-locked entangled state with selected frequencies and a distinct temporal profile, causing a revival for every possible temporal output mode of the cavity. Assuming the cavity contains a single excitation, the intensity of the output field is exponentially decaying and thus results in a diminished visibility of the interference for longer delay times. A cavity around a single photon source produces the same effect and enhances the photon rate. To date, this effect has only been demonstrated over the range of several centimeters and a maximum of nine revivals [24].

Here, we present the first source that produces nonclassical interference for >100 meters path difference between photons, and measure HOM interference out to the 84th revival.

Biphoton frequency comb.—We produce frequency-entangled single photon pairs at 795 nm by cavity-enhanced spontaneous parametric down-conversion (SPDC), achieving a spectral brightness of $(4.4 \pm 0.4) \times 10^3$ photon pairs/(s mW MHz) [25]. The pump light at 397.5 nm is generated inside a separate cavity with a linewidth ~3 MHz. We then type-II quasiphase match in a periodically poled potassium titanyl phosphate crystal to obtain the photon pairs. Birefringence is compensated by the flip trick [26]: a half wave plate (HWP) at 45° inside the bow-tie cavity flips the polarization of each down-converted photon once per *physical* round trip of temporal length T_p. Two physical round trips, one in each polarization, become one *effective* round trip, referenced henceforth simply as round trip with $T \equiv 2T_p$.

The biphoton frequency comb spans the 100 GHz full width at half maximum phase-matching bandwidth of the crystal and thus contains approximately 800 frequency modes, spaced by 120.8 MHz—the free spectral range (FSR) of the cavity. As signal and idler photons satisfy the resonance condition simultaneously, the linewidth of the frequency modes are smaller than the width of the cavity
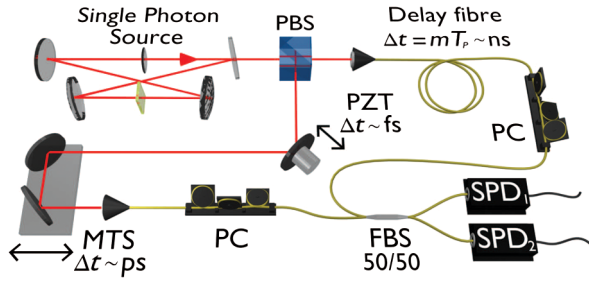
FIG. 1. Schematic showing methods for coarse, intermediate, and fine photon delays before the 50/50 fiber beam splitter (FBS). PBS, polarizing beam splitter; $m \in \mathbb{N}_0$; T_p, physical round trip time; PZT, piezoelectric transducer; PC, polarization controller; MTS, motorized translation stage; SPD, single photon detectors. *Coarse* (right top): optical fibers provide delays on the scale of multiple round trips; *Intermediate* (left lower corner): the motorized translation stage allows scanning over nanosecond ranges; *Fine* (center): wavelength scale resolution is achieved with the scanning piezo controller.

resonance [27], which are 429 ± 10 kHz for the modes and 666 ± 15 kHz for the cavity, respectively [26,28]. This corresponds to a coherence time for the heralded single photons of $\tau_{\rm coh} = 740 \pm 20$ ns [25], enabling the observation of quantum effects between two photons with temporal delays up to this magnitude.

We implement temporal delays for our experiments through a combination of different methods, as shown in Fig. 1. *Coarse* delays select which HOM dip is observed, *intermediate* delays allow scanning over individual dips, and *fine* delays enable observation of subwavelength scale features. Coarse delays are introduced by the addition of optical fibers matched to multiples of the physical cavity round trip time of $T_p = T/2 = 4.14$ ns ($\sim$meters). Intermediate delays are on the order of picoseconds ($\sim$millimeters), achieved in free-space with two mirrors on a motorized translation stage before the photons are coupled into fiber. Fine delays on the order of femtoseconds ($\sim$nm) are achieved using a piezo-mounted mirror.

Quantum interference with a biphoton frequency comb.—Down-conversion in our source can be described using the standard interaction Hamiltonian for SPDC of type II [29]. In our case, this Hamiltonian leads to results differing from those found in [27,30]: the flip trick changes the photons' polarization with each physical round trip. Therefore, the two photons can be detected in either the *even comb*, where the photons have orthogonal polarization and a detection time difference δt equal to even multiples of the physical cavity round trip time ($T_p^e \equiv 2nT_p$, $n \in \mathbb{N}_0$); or the *odd comb*, where the photons have the same polarization and a time difference equal to odd multiples [$T_p^o \equiv (2n + 1)T_p$]. This results in the state,

$$|\psi\rangle \propto \sqrt{2}|1_{\rm H}1_{\rm V}\rangle_{\delta t = T_p^e} + (|2_{\rm H}0_{\rm V}\rangle + |0_{\rm H}2_{\rm V}\rangle)_{\delta t = T_p^o}. \quad (1)$$

Note that the temporal structure eliminates overlap between the $|1_{\rm H}1_{\rm V}\rangle$ and $|2_{\rm H}0_{\rm V}\rangle/|0_{\rm H}2_{\rm V}\rangle$ terms, regardless of the photons' polarization. However, each state component in Eq. (1) is in itself a frequency-entangled, two-photon state containing a superposition of amplitudes for all possible even (odd) detection time differences.

The signals from detectors 1 and 2 shown in Fig. 1 are used to obtain the integrated coincidence signal, $\bar{G}_{1,2}^{(2)}(\Delta t)$, where Δt is the temporal delay between the photons before the beam splitter. Averaging the Glauber cross-correlation function over all possible detection times yields

$$\bar{G}_{1,2}^{(2)}(\Delta t) = \frac{1}{4}(1 - f(2\Delta t)) + \frac{1}{2}\sin^2(\omega_0 \Delta t), \quad (2)$$

where f is a function of the temporal amplitude of the photons and ω_0 is the central single photon frequency. The two distinct contributions in this cross-correlation function arise respectively from the even and odd frequency combs.

The first term of Eq. (2) is due to the even comb—the $|1_{\rm H}1_{\rm V}\rangle$ state—and describes the resulting destructive two-photon interference at the 50/50 beam splitter. It contains the only dependence of $\bar{G}_{1,2}^{(2)}(\Delta t)$ on the temporal amplitude of the two-photon state, via the function

$$f(2\Delta t) = e^{-2\pi\gamma|\Delta t|}(1 + 2\pi\gamma|\Delta t|)\sum_m h(2(\Delta t - mT_p)).$$
$$(3)$$

Here γ is the cavity linewidth, h is the dip shape dependent on the filters in the setup, and $m \in \mathbb{Z}$. This shows that the photons not only interfere destructively around zero delay, but also at delays which are an integer multiple of the physical round trip time T_p caused by the cavity. The shape of each separate dip is identical to the shape $h(t)$ observed in absence of the cavity function.

The second term in Eq. (2) is the result of the odd comb— the two-photon NOON-state [19,20] component. Here, the delay Δt does not change the detection time difference of the two photons, but introduces a relative phase $\varphi \propto \omega_0 \Delta t$. The beam splitter translates this relative phase into oscillations of the NOON state: $\varphi = 0$ leaves it unaffected while $\varphi = \pi$ transforms into the $|11\rangle$ state at the output.

In our experiment, the photons are separated deterministically after the cavity with a polarizing beam splitter (PBS) before being coupled into single mode fiber. HOM interference occurs at a 50/50 fiber beam splitter (FBS), with polarization control on both input ports. The two outputs are connected to silicon avalanche photon detectors and their signals recorded with a time-tagging module, Fig. 1.

Even-comb quantum interference.—Fig. 2(a) shows the central HOM dip originating from the even-comb contributions in Eq. (1) as the photon delay varies over a timescale of tens of picoseconds (intermediate delay). Similar traces
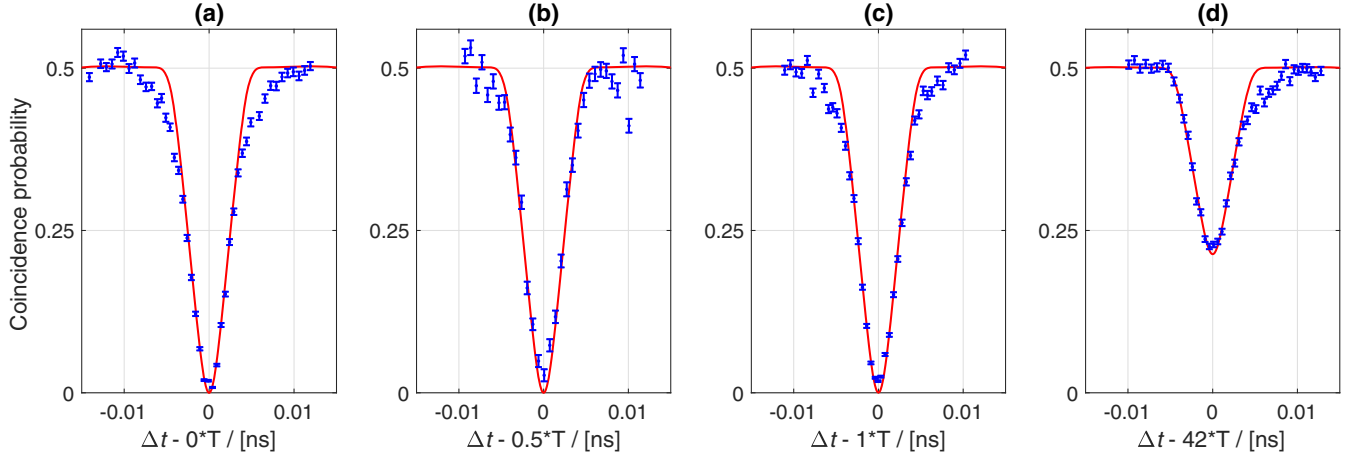
FIG. 2. Coincidence probability of even-comb photons in a HOM interference experiment for selected coarse time delays $\Delta t \propto T (=8.28$ ns), data in blue, theory in red. Error bars are dominated by the uncertainty in the coincidence counts. Delays are introduced by a set of optical fibers of length 0, ½, 1, and 42 round trips, corresponding to a free space path differences up to 105 m between the photons. Intermediate time delays between data points within (a)–(d) are achieved with a pair of mirrors mounted on a motorized translation stage with step sizes between 0.5–1.3 fs (150–400 μm). See Supplemental Material [31] for additional plots.

at positions selected with coarse delays achieved by combining fibers equivalent to ½, 1, and 42 round trip times are shown in Figs. 2(b)–2(d) (additional dips at 2, 4, and 40 round trip times and a detailed description of the procedure for collecting and post-processing of the data can be found in the Supplemental Material [31]). The data points (blue) agree well with the fully constrained theoretical model (red), where the model parameters are experimentally determined values for linewidth, FSR, phase matching envelope, and implemented narrow-band filters in Eq. (2) at constant phase. The visibility of HOM interference is given by $V = (P_{max} - P_{min})/P_{max}$, with $P_{min(max)}$ the minimal (maximal) coincidence probability. At zero time delay we observe near-ideal visibility, $V = (98.4 \pm 1.7)\%$.

When single photons arrive from either side of the 50/50 beam splitter, the cases where either both photons are transmitted (tt) or reflected (rr) interfere destructively, giving rise to the HOM dip [2], Fig. 2(a). All temporal components of the even-comb biphoton state overlap as shown in Fig. 3(a), and thus interfere. If a temporal delay Δt is introduced, the tt and rr detection probability amplitudes are both shifted, however, in opposite directions. This leads to a relative shift of $2\Delta t$ so that the amplitudes reoverlap for delays matching an integer multiple of $T/2$, $\Delta t = m * T/2$ with $m \in \mathbb{Z}$, as illustrated in Fig. 3(b), resulting in HOM dip revivals, Figs. 2(b)–2(d). We emphasize that the somehow counterintuitive revival period is ensured by the temporal entanglement of the two photons.

The relative shift of the biphoton detection amplitudes lowers their quantitative overlap—especially visible around the center of Fig. 3(b)—which further decreases with increasing temporal shift. This mismatch subsequently reduces the visibility of the interference as illustrated in Fig. 4 (see Supplemental Material [31] for table of visibility

values). The small discrepancies between the measured data and theoretical predictions in Fig. 4 arise from residual distinguishability in the polarization d.o.f., and from the beam splitter reflectivity varying slightly from 50%. Observing the HOM dips with hundreds-of-nanosecond delays is proof of the long coherence time and narrow linewidth of our photons, while requiring the matching arrival times of the photons on the picosecond scale demonstrates the mode-locked state of the generated photon pairs.
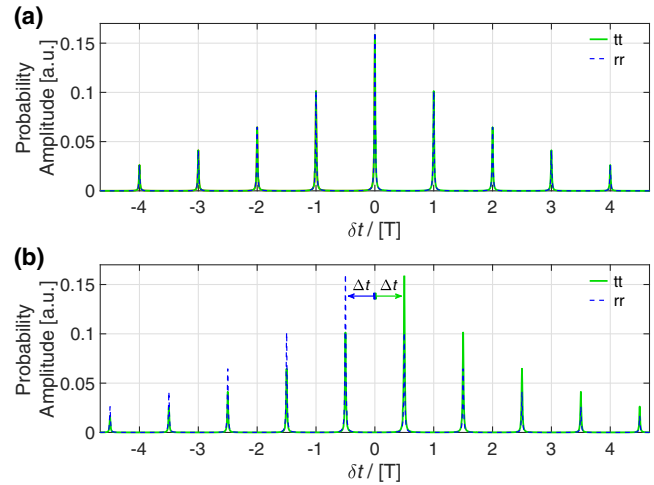

FIG. 3. Detection probability amplitudes of the reflected-reflected (rr) and transmitted-transmitted (tt) photon paths in the HOM experiment. (a) No temporal delay, $\Delta t = 0$. Amplitudes cancel each other out perfectly. (b) Revivals occur when the photons are delayed by $\Delta t = mT_p = m * T/2$ ($m \in \mathbb{Z}$), here shown for $m = 1$. Both detection probability amplitudes shift by the implemented delay but in opposite directions, overlapping the combs again.
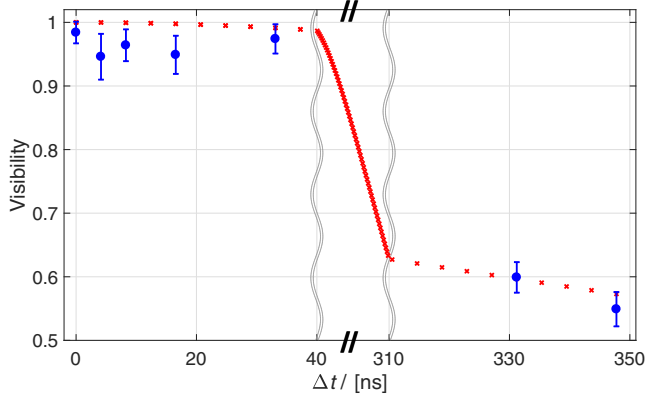
FIG. 4. HOM interference visibilities as a function of coarse round trip delays. Experimental data (blue) and theoretical predictions (red) for 0, ½, 1, 2, 4, 40, and 42 RT delays. Error bars capture the uncertainties in the photon detection and counting modules.

Odd-comb quantum interference.—The integrated single photon count rate of each individual detector,

$$\bar{G}_{1/2}(\Delta t) = 1 \pm \cos(\omega_0 \Delta t) e^{-\pi\gamma|\Delta t|}(1 + \pi\gamma|\Delta t|)$$
$$\times \sum_{m \text{ odd}} h(\Delta t - mT_p), \qquad (4)$$

oscillates with the relative delay Δt. This results from the interference of the probability amplitudes corresponding to

the $|1_H 1_V\rangle$ and $|2_H 0_V\rangle + |0_H 2_V\rangle$ components of the state, which is only visible at delays close to odd multiples of T_p. To understand this, note that originally the detection time difference of the two photons is an even (or odd) multiple of the physical cavity round trip time for the $|1_H 1_V\rangle$ (or $|2_H 0_V\rangle + |0_H 2_V\rangle$) state component. In principle, these contributions can be distinguished and no interference takes place. However, as the delay Δt only affects the detection time difference for the $|1_H 1_V\rangle$ component, the two contributions become indistinguishable if $\Delta t \approx T_p^o$, and interference is observed. The visibility of the oscillations in Eq. (4) maximizes at the center of the half-round trip HOM dip, where the even and odd comb cannot be distinguished temporally. The interference itself is modulated across twice the width of the HOM dip as for first-order interference Δt only enters once in the relative shift of the probability amplitudes.

We emphasize that this is the result of first-order interference between the odd and even comb and consequently has to be distinguished from the oscillation of $\bar{G}_{1,2}^{(2)}(\Delta t)$ in Eq. (2), which is a result of the second-order interference of only the contributions from the NOON state.

To record these fast nanometer-scale oscillations, we require time delays with femtosecond precision that are implemented with a mirror mounted on a piezoelectric transducer (PZT). Oscillations at selected points can be seen in Figs. 5(b)–5(f), with their corresponding position
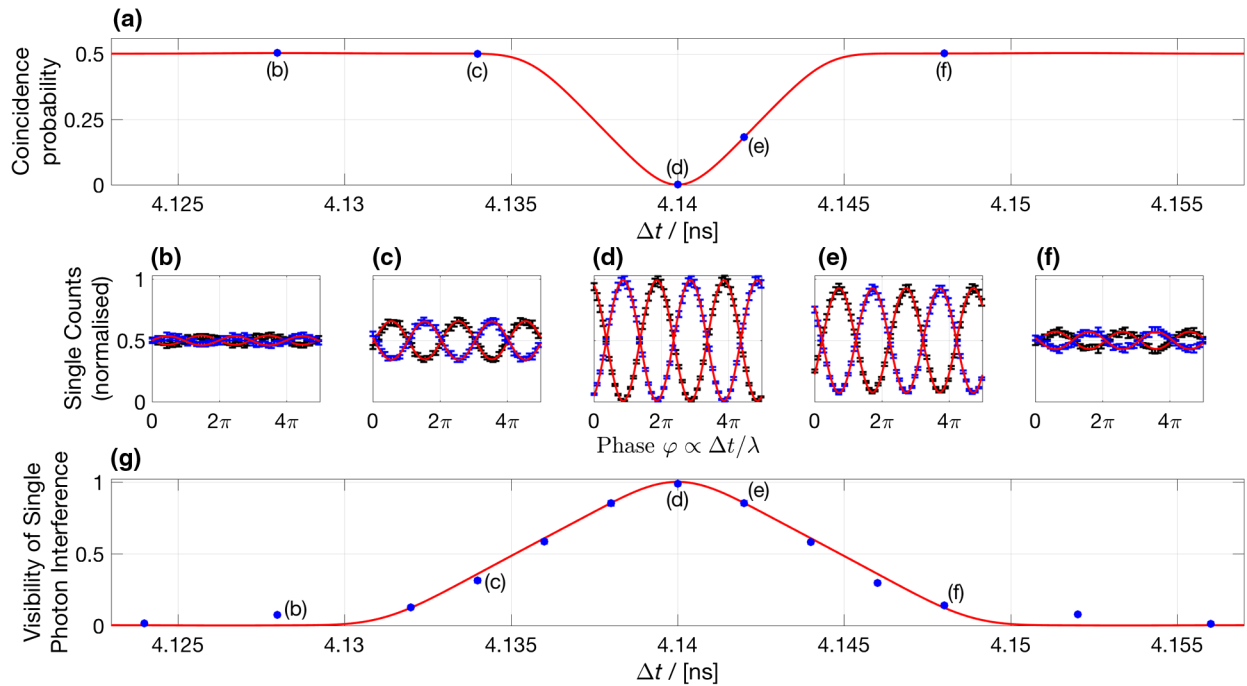

FIG. 5. Single photon interference. (a) Theoretical coincidence probability between the two detectors (=HOM dip) at $\Delta t = T/2$ in order to indicate the rough positions used to obtain the oscillations shown in (b)–(f). The delay is implemented with a set of mirrors mounted on a translation stages, see Fig. 1. (b)–(f) The oscillations of the single photon counts on the two detectors in blue and black, respectively. The fit in red illustrates the expected periodicity of one wavelength and a maximal visibility for (d), at the bottom of the dip. The phase delay is realized by a mirror mounted on a piezoelectric transducer. (g) Interference visibilities, data in blue with error bars smaller than the dots, theory in red. Captions next to the data correspond to the relevant oscillation and positions on the HOM dip.

on the HOM dip around $T/2$, Fig. 5(a). Following Eq. (4), the expected visibilities are compared to the measured results in Fig. 5(g) (the plots of all oscillations are presented in the Supplemental Material [31]). Comparing Figs. 5(a) and 5(g) clearly illustrates the expected broader range of single oscillations, with visibilities up to 0.5 outside the actual HOM dip.

Discussion.—We demonstrate the first nonclassical interference between photons delayed by more than ⅓ of a microsecond—equivalent to 105 meter path length difference—measuring a visibility of 55% at that delay, 96% of the theoretically predicted value. Therefore, this source can naturally be exploited in quantum networks based on time resolved correlation measurements [32,33], including multi-boson correlation sampling schemes [34,35]. Additionally, our source achieves a heretofore unachieved spectral brightness of $(4.4 \pm 0.4) \times 10^3$ photon pairs/smWMHz.

The source is a novel metrological tool that exhibits different kinds of quantum interference depending on which frequency comb is temporally accessed—a quantum brush if you will. By experiencing HOM interference with phase-sensitive NOON-state superresolution fringes at $2\omega_0 \Delta t$, and simultaneously singles oscillations at $\omega_0 \Delta t$—with twice the spatial or temporal displacement range as the HOM interference—our source allows enhanced precision in distance sensing of subwavelength features in a quantum-secured way. The HOM interference will vanish if the state of either photon is altered, allowing applications such as establishing a quantum-secured optical perimeter. Furthermore the entangled frequency combs in our source are a promising resource for frequency-multiplexed quantum information processing [36,37].

*mrks.rambach@gmail.com

[1] Z. Ou, C. Hong, and L. Mandel, Opt. Commun. **63**, 118 (1987).

[2] C. K. Hong, Z. Y. Ou, and L. Mandel, Phys. Rev. Lett. **59**, 2044 (1987).

[3] Y. H. Shih and C. O. Alley, Phys. Rev. Lett. **61**, 2921 (1988).

[4] E. Knill, R. Laflamme, and G. J. Milburn, Nature (London) **409**, 46 (2001).

[5] J. L. O'Brien, G. J. Pryde, A. G. White, T. C. Ralph, and D. Branning, Nature (London) **426**, 264 (2003).

[6] N. K. Langford, T. J. Weinhold, R. Prevedel, K. J. Resch, A. Gilchrist, J. L. O'Brien, G. J. Pryde, and A. G. White, Phys. Rev. Lett. **95**, 210504 (2005).

[7] P. Kok, W. J. Munro, K. Nemoto, T. C. Ralph, J. P. Dowling, and G. J. Milburn, Rev. Mod. Phys. **79**, 135 (2007).

[8] J. L. O'Brien, A. Furusawa, and J. Vučković, Nat. Photonics **3**, 687 (2009).

[9] J.-W. Pan, D. Bouwmeester, H. Weinfurter, and A. Zeilinger, Phys. Rev. Lett. **80**, 3891 (1998).

[10] P. G. Kwiat and H. Weinfurter, Phys. Rev. A **58**, R2623 (1998).

[11] G. J. Pryde, J. L. O'Brien, A. G. White, S. D. Bartlett, and T. C. Ralph, Phys. Rev. Lett. **92**, 190402 (2004).

[12] M. A. Broome, A. Fedrizzi, S. Rahimi-Keshari, J. Dove, S. Aaronson, T. C. Ralph, and A. G. White, Science **339**, 794 (2013).

[13] J. B. Spring, B. J. Metcalf, P. C. Humphreys, W. S. Kolthammer, X.-M. Jin, M. Barbieri, A. Datta, N. Thomas-Peter, N. K. Langford, D. Kundys, J. C. Gates, B. J. Smith, P. G. R. Smith, and I. A. Walmsley, Science **339**, 798 (2013).

[14] M. Tillmann, B. Dakić, R. Heilmann, S. Nolte, A. Szameit, and P. Walther, Nat. Photonics **7**, 540 (2013).

[15] A. Crespi, R. Osellame, R. Ramponi, D. J. Brod, E. F. Galvão, N. Spagnolo, C. Vitelli, E. Maiorino, P. Mataloni, and F. Sciarrino, Nat. Photonics **7**, 545 (2013).

[16] P. Chen, C. Shu, X. Guo, M. M. T. Loy, and S. Du, Phys. Rev. Lett. **114**, 010401 (2015).

[17] D. A. Kalashnikov, E. V. Melik-Gaykazyan, A. A. Kalachev, Y. F. Yu, A. I. Kuznetsov, and L. A. Krivitsky, Sci. Rep. **7**, 11444 (2017).

[18] A. Lyons, G. C. Knee, E. Bolduc, T. Roger, J. Leach, E. M. Gauger, and D. Faccio, Sci. Adv. **4** (2018).

[19] H. Lee, P. Kok, and J. P. Dowling, J. Mod. Opt. **49**, 2325 (2002).

[20] J. P. Dowling, Phys. Rev. A **57**, 4736 (1998).

[21] K. J. Resch, K. L. Pregnell, R. Prevedel, A. Gilchrist, G. J. Pryde, J. L. O'Brien, and A. G. White, Phys. Rev. Lett. **98**, 223601 (2007).

[22] L. Schwarz and S. J. van Enk, Phys. Rev. Lett. **106**, 180501 (2011).

[23] Y. J. Lu, R. L. Campbell, and Z. Y. Ou, Phys. Rev. Lett. **91**, 163602 (2003).

[24] Z. Xie, T. Zhong, S. Shrestha, X. Xu, J. Liang, Y.-X. Gong, J. C. Bienfang, A. Restelli, J. H. Shapiro, W. N. C., and C. W. Wong, Nat. Photonics **9**, 536 (2015).

[25] M. Rambach, Ph.D. thesis, University of Queensland (2017).

[26] M. Rambach, A. Nikolova, T. J. Weinhold, and A. G. White, APL Photonics **1**, 096101 (2016).

[27] M. Scholz, L. Koch, and O. Benson, Opt. Commun. **282**, 3518 (2009).

[28] M. Rambach, A. Nikolova, T. J. Weinhold, and A. G. White, APL Photonics **2**, 119901 (2017).

[29] M. H. Rubin, D. N. Klyshko, Y. H. Shih, and A. V. Sergienko, Phys. Rev. A **50**, 5122 (1994).

[30] U. Herzog, M. Scholz, and O. Benson, Phys. Rev. A **77**, 023826 (2008).

[31] See Supplemental Material at http://link.aps.org/supplemental/10.1103/PhysRevLett.121.093603 for further theoretical derivations, details on the data collection procedure and additional plots.

[32] V. Tamma and S. Laibacher, Phys. Rev. Lett. **114**, 243601 (2015).

[33] S. Laibacher and V. Tamma, arXiv:1706.05578.

[34] S. Laibacher and V. Tamma, Phys. Rev. Lett. **115**, 243605 (2015).

[35] S. Laibacher and V. Tamma, arXiv:1801.03832.

[36] H.-H. Lu, J. M. Lukens, N. A. Peters, O. D. Odele, D. E. Leaird, A. M. Weiner, and P. Lougovski, Phys. Rev. Lett. **120**, 030502 (2018).

[37] J. M. Lukens and P. Lougovski, Optica **4**, 8 (2017).